RESEARCH ARTICLE

Application of Active Electric Field in Defect Detection

Wenjie Yang[1], Jiegang Peng[2]*, Lin Xu[3], Jiaqi Wang[4]

[1,2,4]*School of Automation Engineering, University of Electronic Science and Technology of China, Xiyuan Street 2006, Chengdu, 610054, People's Republic of China*
[3]*Wuhan Second Ship Design and Research Institute, Wuhan, 430202, People's Republic of China*

*Corresponding author: E-mail: pjg2000cn@hotmail.com

Inspired by the research on the active electrolocation organs of weakly electric fish in bionic engineering field, we proposed a new defect detection method based on the active electric field detection principle. In this study, we established an underwater defect detection experimental platform, and conducted joint time-frequency analysis and recognition algorithm on electric field signals collected during the experiment to obtain the joint time-frequency spectrogram (JTFS) and frequency inflection points (FIPs) of the detected objects. Through the JTFS and FIP of the tested object, we can get the defect size and position information and carry out further data processing in deeper exploration. This new defect detection method not only increases the types of defect detection methods, but also broadens the application range of active electric field. The study starts from the perspective of engineering experiments and demonstrates the feasibility and effectiveness of the novel defect detection method.

Introduction

The idea of active electric field detection originated from bionics research. Since the 1950s, biological researchers have found a kind of fish in the river of Amazon basin. This kind of fish emits low frequency weak electric field with amplitude of about 1V and frequency no more than 1000Hz through its own discharge tissues (EODs, electric organ discharges). When the electric field spreads in water, if there is an object in the propagation path, the spatial distribution of the electric field in the water will be distorted. This kind of fish will obtain the distorted electric field information through the electric field sensing organ to guide its own life activities. That's why scientists call them weak electric fish.

The researchers' experiments found that the electric field sensing organs of weakly electric fish can accurately detect changes in electric field amplitude by 1%. By means of electric field emission organs and sensing organs, weak electric fish can evade hunting, predation, navigation and positioning. The researchers named this detection method underwater active electric field localization. Based on this biological mechanism, weak electric fish can survive in completely dark and murky water and can perceive the surrounding environment in an all-round way to obtain comprehensive environmental information such as the location, size, shape and composition of surrounding objects [1].

Many research studies have been performed to deeply understand the active electric field positioning mechanism

of weakly electric fish and there have been more engineering exploration and application in the past 20 years. In 1998, Caputi *et al.* found that the change of electric field information of weakly electric fish is related to the conductivity of the medium and objects in the surrounding environment. In the same year, Nelson *et al.* and MacIver *et al.* demonstrated that the change is also related to the electrical characteristics of objects and the distance between objects and weakly electric fish [2-4]. In 2003, the influence of several objects on the active electrolocation system of weakly electric fish was studied by Adriana Migliaro *et al.* The results demonstrated that the electric field information was not a simple linear overlay of each object, but the electric fields affected each other when multiple objects surrounded the fish [5]. In fact, there are many factors that affect the electrical image: The volume of the object, some physical and chemical characteristics of the object, the distance of the object from the weakly electric fish, the conductivity of the object, and the conductivity of the medium environment [6-8]. In 2003, Lebastard *et al.* practically applied it to underwater active electrolocation and tried to measure the size of the object [9]. In 2004, active electric field technology was applied to underwater vehicles for the first time, and its rationality was validated [3,10]. In 2008, Solberg *et al.* began to apply it to the positioning of underwater objects [11]. In 2012, Noël Servagent *et al.* developed a sensor model based on underwater active electrolocation [12]. In 2015, Dimble *et al.* proposed and experimentally verified an obstacle

Advanced Materials Proceedings

https://amp.iaamonline.org

IAAM
International Association of
Advanced Materials

www.iaamonline.

avoidance strategy based on active electric field detection [13]. In 2016, Bai *et al.* determined an algorithm that could estimate the size, distance, and shape of prolate spheroids, and they employed an active motion and supervised learning approach that estimates object shape in a sequential manner with a reasonable level of accuracy [14]. In 2019, Fujita *et al.* used different shapes of resistive objects and demonstrated that an integration effect of the peak amplitude and half-maximum width could be an invariant measure of object shape [15]. Gottwald *et al.* designed an electric camera device that probed underwater objects with a weak electric field and captured 'electric images' of the targets [16].

The exploration of the above research mainly focuses on the orientation of electric field, and only a few articles mention object detection and related information acquisition. In these studies, Gottwald *et al.* in Germany successfully applied the principle of active electric field to the object detection direction and proved that the target detection method based on active electric field can effectively detect close-range objects of different materials and sizes [16]. Through their research, we can realize that the active electric field used in object information detection is feasible and one of the important research directions in its future development.

Nowadays, the scale of the submarine pipeline transportation industry is huge. At the same time, the defect detection of submarine pipelines has become more and more important. By timely detection and repair of pipeline defects, sudden failures can be avoided, maintenance costs can be reduced, and pipeline service life can be extended. The above research based on based on active electric field positioning and object detection have made extremely beneficial attempts to promote the application of active electric field detection in different test scenarios, and provided us with important inspirations: it is feasible and effective to use active electric field technology to detect objects and obtain relevant information, especially defect information. The defect detection method studied in this paper is expected to become a new underwater pipeline defect detection method and be applied. And with the existing more mature defect detection technology to form a complementary advantage, such as its simple operation, without the need for underwater visual inspection as on the need for professional divers to operate, compared with ultrasonic detection technology [17,18], is not easy to be interfered with by the underwater environment, but also do not need to be like the use of magnetic particle detection technology [19,20] before the use of the object to be measured for surface cleaning. Therefore, we deeply study the defect detection method based on active electric field, and explore the effectiveness of defect detection from the perspective of engineering experiment.

Theory

The theory of this paper mainly starts from the excitation polarization effect, which refers to the fact that under the action of the excitation field, substances with different electrochemical properties will produce a secondary electric field that changes with time due to electrochemical action. As shown in the **Fig. 1**, under the action of the excited electric field, the voltage signal generated by the object due to the excited polarization effect will change with time.
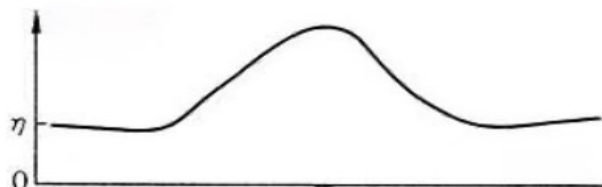

Fig. 1. Variation with time of the electric field produced by the excitation polarization effect

When a weakly electrified fish is surrounded by conductive objects, the amplitude and phase of the signal perceived by the fish's electroreceptive organs change [17]. FIP phenomena based on active electric field cannot be explained by electromagnetic field theory because when a conductor is present in an underwater electric field, the frequency-dependent behavior of conductivity becomes apparent, and the magnitude of the complex impedance of the object changes with the frequency of the excitation signal, and at a certain frequency, the change in the electric field caused by the excitation-excitation effect is minimized, and this frequency is frequency inflection points.

In 2015, researchers discovered the amplitude-frequency response of different electric field frequencies to detected objects in underwater active electric electrolocation systems, and proposed the frequency inflect point (FIP) of amplitude-frequency information characteristics (AIFC). This AIFC study played a significant role in researching the relationship between an object's features and active electric field emission signals [18]. By comparing the FIPs of probed objects made of three different materials and in two different shapes, researchers found that the shape of the probed object had a significant effect on the FIP of the AIFC for the active electrolocation system. In 2017, Based on the research in 2015, Peng established an equivalent circuit model of the underwater active electrolocation system, which provides theoretical guidance for our research [19,20].

As **Fig. 2** depicts, parallel conduction through a purely resistive element is simulated by the resistance R_0, $R_{Trans}(\omega)$ is the equivalent impedance of the transmitting electrode, and $R_{Recv}(\omega)$ is the equivalent impedance of the receiving electrode. When there is no object in the water (**Fig. 1(a)**), the measured voltage is expressed as U_{Object}. When the probed object is directly below the detection electrodes (**Fig. 1(b)**), R_{Object} is the equivalent impedance of the probed object and its IP effect. $R_{Saltwater}$ is the equivalent impedance of the water that is drained by the probed object. The measured voltage is expressed as U_{free}.
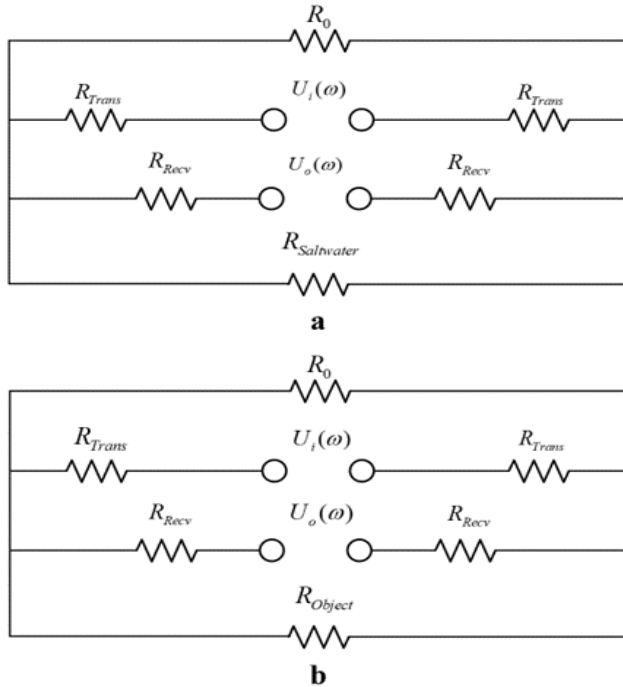
Fig. 2. Equivalent circuits for the underwater active electrolocation system with and without an object in the vicinity.(a) Circuit without object. (b) Circuit with object.

If the equivalent impedance of the measured area is greater than the impedance of the same volume of water, $\Delta U = U_{Object} - U_{free} > 0$. Thus, when the electrode scans the probed object, the AIFC exhibits a convex shape, defined as the positive characteristic. If the equivalent impedance of the measured area is smaller than the impedance of the same volume of water, $\Delta U < 0$ and the AIFC exhibits a concave shape, defined as the negative characteristic. Specifically, when the probed object has an IP effect, its AIFC will exhibit positive characteristics for lower frequency excitation and negative characteristics for higher frequency excitation. At a particular frequency in between, the AIFC will exhibit neither positive nor negative characteristics. This particular frequency is f_{FIP} and the electric field distortion is minimum when the frequency of electric field signal is equal to f_{FIP} [19,20].

Experimental

In order to conduct defect detection experiments, we built an underwater active electric field experimental platform based on the principle of active electrolocation of weakly electric fish. The platform mainly included 4 parts: An experiment detected environment, a sensor probe module, a motion module, and a data processing module. The experimental environment was a 90cm*57cm*40cm water tank. During the experiment, the object under test was kept completely submerged in the water, and the front ends of the transmitting and receiving electrodes were below the horizontal plane. The experiment was carried out at room temperature, in order to simulate the seawater environment,

the conductivity of water was maintained at 5.91 mS / cm by adding NaCl in the experiment. The sensor probe module includes a pair of transmitter electrodes and a pair of receiver electrodes, as well as a holder for mounting the electrodes. The transmitting electrode was used to establish the underwater active detection electric field, and the receiving electrode was used to collect the disturbed electric field signal. The distance between two transmitting electrodes was 7.5 cm, and the distance between two receiving electrodes was 5.6 cm. The four electrodes are all made of titanium alloy with a resistivity of 1.75×10^{-8} Ω•m.

The motion module is a three-axis motion system that controls the movement of the probe module in three-dimensional space by means of motors and rails to realize data acquisition. In the experiment, the operation control module controlled the sensor probe to move from left to right along the X-axis. The movement speed was set to 3 mm/s to ensure adequate sampling points were obtained for each waveform. In this experiment, we used the signal generator HDG2102B as the signal source of the transmitting electrode, and an NI USB-6289 data acquisition (DAQ) board was used to collect data from the receiving electrodes. Data processing was done using specialized data processing software, DIAdem and Origin. The experimental platform and overall structure are shown in **Fig. 3**, and the structure of the sensor probe module is shown in **Fig. 4**.
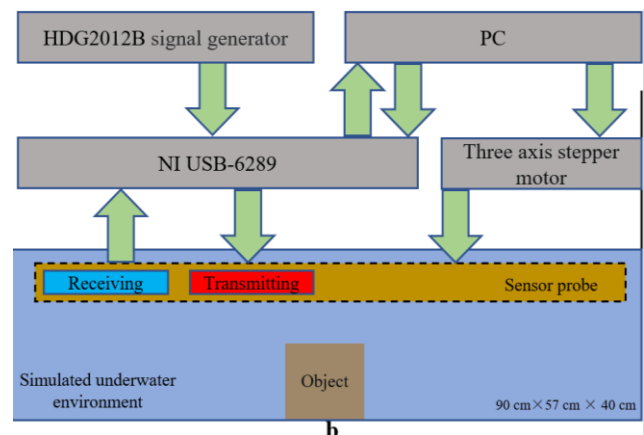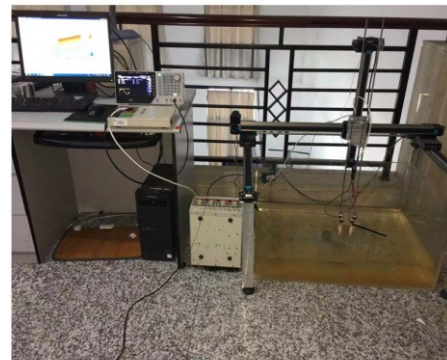

Fig. 3. Experimental bench general view and overall structure. (**a**) Experimental bench general view. (**b**) Overall structure of the platform.

Advanced Materials
Proceedings

https://amp.iaamonline.org

IAAM®
International Association of
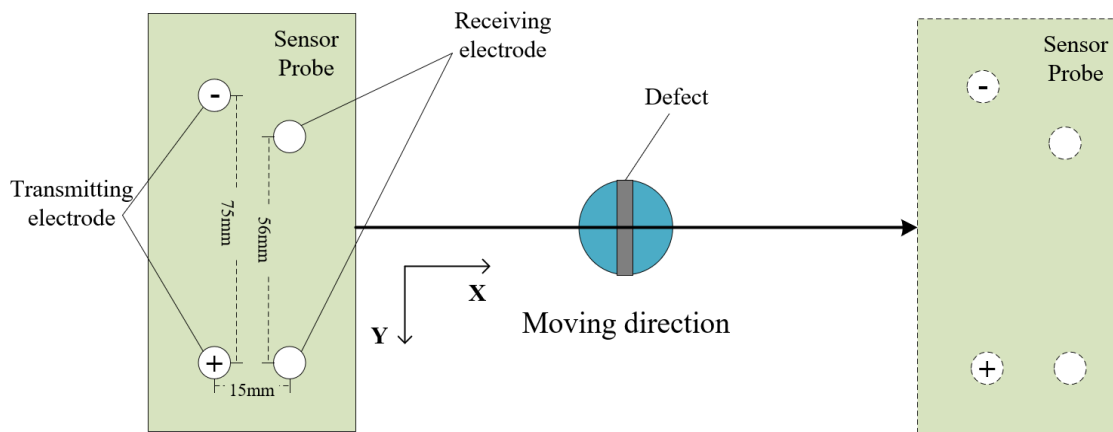Advanced Materials

www.iaamonline.

Fig. 4. Schematic of the sensor probe module and experimental setup for the underwater active electrolocation system.

By performing a short time Fourier transform on the collected data, a joint time spectrogram is plotted using the software, where the x-axis represents the frequency, the y-axis represents the time, and the z-axis represents the amplitude, and the whole spectrogram is the variation of amplitude with time at different frequencies. (That is, the change of amplitude with position)

This study focuses on the feasibility and effectiveness of applying FIP phenomena to defect detection. Therefore, we need to study the changes of FIP under different defect conditions of different materials. In order to simplify the experiment, we keep other experimental conditions that may affect the detection results unchanged and only change the test object during the experiment. During the experiment, the sensor probe needs to be immersed in water and move at a constant speed on the detected target object. Then the AIFC of the distorted electric field collected by each experiment is transformed into the frequency domain for analysis and processing. The sensor probe moves at a constant speed of 6cm/s along the X-axis direction of the current target object, and obtains an energy density matrix P data point every 3s. After collecting a set of data, it is necessary to replace the measured object for experiment, so as to obtain the original information data of different measured objects. In the experiment, the square wave with a frequency of 20Hz, peak-to-peak value of 2v and duty cycle of 50% is used as the transmitting signal, and the sampling frequency is 10000hz. The detected objects are 50×50mm copper cylindrical objects. The tested objects have different defect conditions, so that enough data can be obtained.

Results and discussion

We selected the most common copper materials to carry out a detailed introduction and analysis of the defect detection process. In the experiment, we selected the detected copper cylinder with different crack sizes, and kept the scanning device moving at a constant speed. In this case, the Y-axis was not only used as a time axis, but also could be used as the position axis of the scanned object according to the time point information and movement speed. Under a single measurement signal frequency, we obtained the JTFS of standard part with crack size of 0mm through experiments. **Fig. 5(a)**, **Fig. 5(b)** and **Fig. 5(c)** are the JTFS at the transmitting signal frequency of 60Hz, 220Hz and 420Hz respectively. In **Fig. 5(a)**, the X-axis represents the frequency distribution of the received signal (Hz), the Y-axis represents the time of the detection device during operation (s), and the Z-axis represents the peak amplitude of the signal after the Fourier transform (dB).
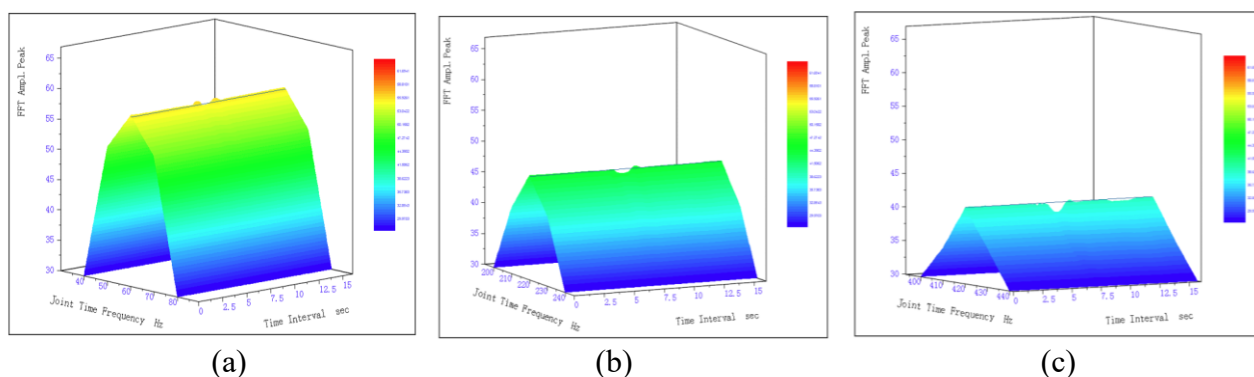

(a)   (b)   (c)

Fig. 5. Single-frequency JTFS of standard copper cylinder (**a**)60Hz. (**b**) 220Hz. (**c**)420Hz

In calculating the FIP, the experimental data were first obtained from the tdms file, and the energy spectral density matrix (the datamization of the top view of the JTFS) was obtained through the DIAdem software; the degree of change of each frequency in the frequency array was then determined by the calculation. For a certain frequency, first find the position of that frequency in P, calculate the average avg over the entire time course, and then obtain the maximum max and minimum min of that frequency component in P during the acquisition process, noting h = (max-avg) - (avg-min) as the degree of aberration. Finally, a polynomial is fitted to the h-f curve. Its zero point is the FIP of the object to be measured.

In **Fig. 5**, each JTFS is in a horizontal state at the beginning and end of a period of time, which is the situation when the detection platform has not touched the detected object, and when it is close to the detected object, the image presents a convex - concave - convex situation, according to which we determine the position of the object. At 60Hz, the overall image presents a convex, basically no depression. At 220Hz, the protrusion and depression of the whole image reach a basic equilibrium state. At 420Hz, the dented part of the image is obviously stronger than the raised part. It can be seen that with the increase of frequency, there is indeed more obvious dented information near the copper cylinder. The detection results are in agreement with the FIP research results proposed by Peng.

For each detected object, we changed the signal frequency and conducted multiple sets of experiments to obtain multiple single-frequency JTFS as shown in Fig. 4. The JTFS at different frequencies are connected in frequency order to form the JTFS of the measured object at multiple frequencies. For copper materials, we used 50 × 50mm cylinders with crack sizes of 0mm, 5mm, 15mm, 25mm and 35mm. The corresponding multi-frequency JFTS are shown in **Fig. 6**.
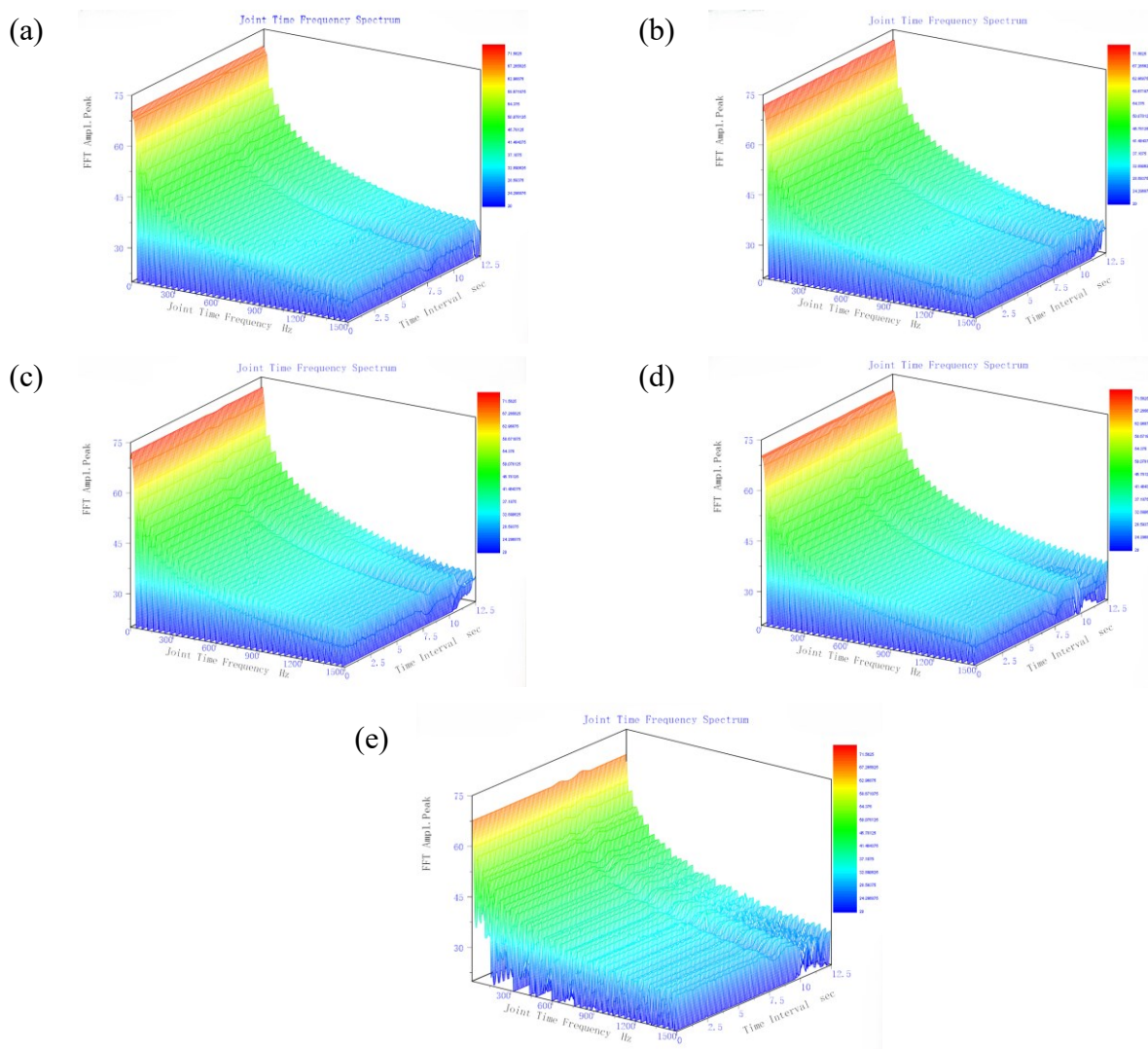

Fig. 6. Multi-frequency JTFS of Copper cylinders with different defect sizes (**a**) Defect 0mm. (**b**) Defect 5mm. (**c**) Defect 15mm. (**d**) Defect 25mm. (**e**) Defect 35mm.

Conclusion

In order to verify the feasibility and effectiveness of underwater active electric field for defect detection, we first conducted experiments on metal objects with IP effect based on the characteristics of FIP. Through a large number of repeated experiments, we obtained the JTFS of copper material under various defect conditions. From Figure 6, it can be obtained that the electric field distortion of the copper cylinder changes with the frequency of the detection signal under different defect conditions. Through JFTS, we can intuitively observe the size and location information of defects, and can see that the FIP of copper cylinders under different defect conditions is increasing. This verifies the validity and feasibility of defect detection based on active electric field principle. The shortcomings of this paper are that more complex defects are not discussed, only a single crack defect is discussed, and there is still a certain distance from the engineering application, but this also lays the foundation for future research, so that we can make a more in-depth exploration.

Conflicts of interest
There are no conflicts to declare.

Keywords: Active electric field, Defect detection, Weakly electric fish.

Supporting information
Supporting informations are available online at journal website.

References

1. D. Rother, A. Migliaro, R. Canetti, *et al.* Electric images of two low resistance objects in weakly electric fish. *J. Biosystems*, **2003**, 71:171-179.
2. A.A. Caputi, R. Budelli, K. Grant, *et al.* The Electric Image in Weakly Electric Fish: Physical Images of Resistive Objects in Gnathonemus Petersii. *J. Journal of Experimental Biology*, **1998**, 201(14): 2115-2128.
3. Maciver, M.A.; Fontaine, E.; Burdick, J.W. Designing future underwater vehicles: Principles and mechanisms of the weakly electric fish. *J. IEEE Ocean. Eng.,* **2016**, 29, 651–659.
4. M E Nelson, M A MacIver. Sensory acquisition in active sensing systems. *J. Journal of Comp. Physiol. A*, **2006**, 192(6): 573-586.
5. Rother, D.; Migliaro, A.; Canetti, R.; Gomez, L.; Caputi, A.; Budelli, R. Electric images of two low resistance objects in weakly electric fish. *J. Biosystems*. **2003**, 71, 169–177.
6. Emde, G.V.D.; Fetz, S. Distance, shape and more: Recognition of object features during active electrolocation in a weakly electric fish. *J. Exp. Biol.* **2007**, 210, 3082–3095.
7. Friedman, J.; Herman, H.; Truong, N.; Srivastava, M.B. A 16-electrode biomimetic electrostatic imaging system for ocean use. *J. IEEE Sens.,* **2011**, 24, 986–989.
8. Emde, G.V.D.; Amey, M.; Engelmann, J.; Fetz, S.; Folde, C.; Hollmann, M.; Metzen, M.; Pusch, R. Active electrolocation in Gnathonemus petersii: Behaviour, sensory performance, and receptor systems. *J. Physiol.-Paris.,* **2008**, 102, 279–290.
9. Lebastard, V.; Chevallereau, C.; Girin, A.; Servagent, N.; Gossiaux, P.B.; Boyer, F. Environment reconstruction and navigation with electric sense based on a Kalman filter. *Int. J. Robot. Res.,* **2013**, 32, 172–188.
10. MacIver, M.A.; Nelson, M.E. Towards a biorobotic electrosensory system. J. *Auton. Robot.,* **2001**, 11, 263–266.
11. Solberg, J.R.; Lynch, K.M.; MacIver, M.A. Active electrolocation for underwater target localization. *Int. J. Robot. Res.,* **2008**, 27, 529–548.
12. Servagent, N.; Jawad, B.; Bouvier, S.; Boyer, F.; Girin, A.; Gomez, F.; Lebastard, V.; Stefanini, C.; Gossiaux, P.B. Electrolocation Sensors in Conducting Water Bio-Inspired by Electric Fish. *IEEE Sens. J.,* **2013**, 13, 1865–1882.
13. Dimble, K.D.; Ranganathan, B.N.; Keshavan, J.; Humbert, J.S. Computationally efficient underwater navigational strategy in electrically heterogeneous environments using electrolocation. In Proceedings of the 2015 IEEE International Conference on Robotics and Automation (ICRA), Seattle, DC, USA, 26–30 May **2015**; pp. 1172–1177.
14. Bai, Y.; Snyder, J.B.; Peshkin, M.; Maciver, M.A. Finding and identifying simple objects underwater with active electrosense. *Int. J. Robot. Res.,* **2016**, 34, 1255–1277.
15. Fujita, K.; Kashimori, Y. Representation of object's shape by multiple electric images in electrolocation. *J. Biol. Cybern.,* **2019**, 113, 239–255.
16. Gottwald, M.; Herzog, H.; Emde, G.V.D. A bio-inspired electric camera for short-range object inspection in murky waters. *J. Bioinspir. Biomim.,* **2019**, 14, 035002.
17. X. Y. Bao. Research on phased array ultrasonic detection system and its key technologies. D. Beijing: Tsinghua University, **2003**.
18. M. J. Jung, B. C. Park, J. H. Bae, *et al.* Paut-Based Defect Detection Method for Submarine Pressure Hull. *J. International Journal of Naval Architecture and Ocean Engineering,* **2018**, 10(2), 153-169.
19. Nikolaos Panagiotopoulos, Robert L Duschka, *et al.* Magnetic particle imaging: current developments and future directions, *International Journal of Nanomedicine,* 10, 3097-3114.
20. Leach, J., & Morris, P. E.; Cognitive Factors in the Close Visual and Magnetic Particle Inspection of Welds Underwater. Human Factors, **1998**, 40(2), 187–197.
21. Bai, Y.; Neveln, I.D.; Peshkin, M.; Maciver, M.A. Enhanced detection performance in electrosense through capacitive sensing. *J. Bioinspir. Biomim.,* **2016**, 11, 055001.
22. Peng, J.G. A study of amplitude information-frequency characteristics for underwater active electrolocation system. *J. Bioinspir. Biomim.,* **2015**, 10, 066007.
23. Peng, J.G.; Wang, Y.L.; Liu, L. A Research on Effect of Probed Object Shape on Frequency Inflection Point (FIP) of Underwater Active Electrolocation System. *J. IEEE Trans. Appl. Supercond.* **2016**, 26, 1–5
24. Ren, Q.X.; Peng, J.G.; Chen, H.J. Amplitude information-frequency characteristics for multi-frequency excitation of underwater active electrolocation systems. *J. Bioinspir. Biomim.,* **2020**, 15, 016004.

Authors Biography

Prof. Jiegang Peng serves as Full Professor for School of Automation Engineering, University of Electronic Science and Technology of China, P.R.C. In 2022, he has been admitted.as Fellow of international Association of Advanced Materials. His current research topics are as fellow: Biomimetic active electrolocation sensor and Electric Field propagation phenomenon in fluid and Mechanism and application of bionic active electrolocation sensor.

Graphical Abstract

Fig. 1 shows the variation of the secondary electric field with time due to the excitation polarization effect. Fig. 2 is the equivalent circuit model of the active potential system. Fig. 3 shows the block diagram of the experimental platform and system structure, which show the equipment required for the experiment. Fig. 4 shows the arrangement of the electrodes and the placement of the object under test. Fig. 5 shows the single-frequency JFTS for a copper cylinder with a defect of 0 mm, and Figs. a, b, and c show the corresponding JTFS for frequencies of 60 Hz, 220 Hz, and 420 Hz, respectively, and Fig. 6 shows the multi-frequency JFTS of copper cylinders with different defect sizes, where Figs. a, b, c, d, and e correspond to defect sizes 0mm, 5mm, 15mm, 25mm, and 35mm, respectively.